Electronic Supplementary Material (ESI) for Dalton Transactions.
This journal is © The Royal Society of Chemistry 2020

Six-Coordinate Mononuclear Dysprosium (III) Single-Molecule Magnets with the Triphenylphosphine Oxide Ligand

Kuduva R. Vignesh,[a] Dimitris I. Alexandropoulos,[a] Haomiao Xie,[a] Kim R. Dunbar [a,*]

Experimental section

General Information

All manipulations were carried out under an inert atmosphere of N_2 using standard Schlenk and glovebox techniques unless otherwise noted. The starting material triphenylphosphine oxide was purchased from Sigma Aldrich, dried under vacuum at 100° C and stored in the glovebox prior to use. Anhydrous $DyCl_3$, $DyBr_3$, DyI_3 and THF without butylated hydroxytoluene as an inhibitor were purchased from Sigma Aldrich and stored under an inert atmosphere. Diethyl ether was purchased from Sigma Aldrich, dried over molecular sieves, distilled and stored over fresh molecular sieves in an inert atmosphere prior to use.

Synthesis of $[Dy^{III}Cl_3(OPPh_3)_2(THF)]\cdot THF$ (1)

Anhydrous $DyCl_3$ (0.23 g, 0.2 mmol) was stirred for 20 minutes in THF (10 mL) and triphenylphosphine oxide (0.21 g, 0.1 mmol) was added with stirring for 30 minutes to yield a yellow solution with precipitate. The solution was filtered and evaporated slowly in one case and in another case and diffused with Et_2O. Crystals of **1** appeared overnight for both methods with an approximate yield of 52% (crystalline product). Anal. Calc. for $C_{40}H_{38}O_3P_2Cl_3Dy$ **(1)**: C, 53.53; H, 4.27 %. Found: C, 53.61; H, 4.18 %. Selected ATR data (Nujol mull, cm^{-1}): 1534 (s), 1413 (m), 1354 (m), 1152 (m), 1125 (w), 1084 (m), 1052 (m), 927 (m), 852 (m), 722 (w), 670 (s), 642 (s), 460 (s).

Synthesis of $[Dy^{III}Br_3(OPPh_3)_2(THF)]\cdot THF$ (2)

The synthesis of **1** was followed, but with anhydrous $DyBr_3$ in place of $DyCl_3$. Crystals of **2** appeared after 2-3 days, in approximate yield of 52% (crystalline product). Anal. Calc. for $C_{40}H_{38}O_3P_2Br_3Dy$ **(2)**: C, 46.60; H, 3.72 %. Found: C, 46.51; H, 3.58 %. Selected ATR data (Nujol mull, cm^{-1}): 1540 (s), 1418 (m), 1346 (m), 1152 (m), 1090 (m), 1048 (m), 930 (m), 842 (m), 718 (w), 665 (s), 640 (s), 462 (s).

Synthesis of [$Dy^{III}I_2(OPPh_3)_4$]I·4THF·0.3H_2O (3)

The synthesis of **1** was followed but with anhydrous DyI_3 being used in place of $DyCl_3$. Crystals of **3** appeared after 2-3 days in an approximate yield of 50% (crystalline product). Anal. Calc. for $C_{72}H_{60}O_4P_4I_3Dy$ **(3)**: C, 52.21; H, 3.65 %. Found: C, 52.32; H, 3.51 %. Selected ATR data (Nujol mull, cm^{-1}): 1540 (s), 1427 (m), 1384 (m), 1120 (m), 1054 (m), 1022 (m), 912 (m), 835 (m), 715 (w), 662 (s), 647 (s), 601, (s), 460 (s).

Single crystal X-ray crystallography. Crystals of **1**·THF**, 2**·THF and **3**·4THF·0.3H_2O were placed in ®Paratone oil and selected under ambient conditions using a MiTeGen microloop. The crystals were placed in a stream of cold N_2 at 110(1) K on a Bruker D8-VENTURE diffractometer equipped with a IμS Cu micro-focus source (λ = 1.54178 Å) for **1**·THF and **2**·THF and a Bruker D8-QUEST diffractometer equipped with a IμS Mo micro-focus source (λ = 0.71073 Å) for **3**·4THF·0.3H_2O. Initial unit cell were determined using SAINT[1] from a set of 3 ω-scans consisting of 30 0.5° frames and a sweep width of 15°. From these unit cell, data collection strategies to collect all independent reflections to a resolution of at least 0.82 Å were implemented using APEX3.[1] Full details of the data collections are presented in Table S1.

For each structure, the data were corrected for absorption using SADABS-2014/5.[2] The space group was determined from analysis of the systematic absences and E-statistics using XPREP. The structures were solved using the intrinsic phasing routine in SHELXT.[3] The non-hydrogen atoms were located from the Fourier difference map and refined using a least-squares refinement algorithm in SHELXL-2014[4] within the OLEX[5] program. All non-hydrogen atoms were refined anisotropically. All hydrogen atoms were placed in calculated positions and refined with thermal parameters constrained to their parent atom. Specific details of the structure refinements are presented below. The programs used for molecular graphics were DIAMOND[6] and MERCURY.[7]

Table S1. Crystal data and structural refinement parameters for compounds **1** – **3**.

Complex	**1**·THF	**2**·THF	**3**·I·4THF·0.3H_2O
Empirical formula	$C_{44}H_{46}DyCl_3P_2O_4$	$C_{44}H_{46}DyBr_3P_2O_4$	$C_{92}H_{100.8}DyI_3P_4O_{10.3}$
Formula weight	969.60	1102.95	2038.4
Temperature/K	100 K	100 K	110 K
Crystal system	Triclinic	Triclinic	Monoclinic
Space group	*P*-1	*P*-1	*P* 21/c
a/Å	11.1577(3)	11.3337(3)	18.5253(8)
b/Å	13.7559 (4)	14.1733(3)	23.7303(10)
c/Å	14.4609(4)	14.5035(4)	20.0073(8)
α/°	83.820(1)	82.893(1)	90
β/°	73.207(1)	72.502(1)	106.966(10)
γ/°	86.080(1)	85.981(1)	90
Volume/$Å^3$	2110.90(10)	2203.58(10)	8412.6(6)
Z	2	2	4
λ / Å	1.54178	1.54178	0.71073
Radiation type	Cu Kα	Cu Kα	Mo Kα
ρ_{calc} / g cm^{-3}	1.526	1.662	1.609
μ / mm^{-1}	12.258	13.257	2.125
Measd / independent (Rint) reflns	39685/7909	35611/8556	134635/15503
Obsd reflns [$I > 2\sigma(I)$]	7747	8218	14606
R_1[a]	0.0232	0.0207	0.0297
wR_2[b]	0.0600	0.0487	0.0739
GOF on F^2	1.077	1.063	1.183
$(\Delta\rho)_{max,min}$ / e $Å^{-3}$	0.576, -0.979	0.382, -0.689	0.950, -1.120

[a] $R_1 = \Sigma(||F_o| - |F_c||)/\Sigma|F_o|$. [b] $wR_2 = [\Sigma[w(F_o^2 - F_c^2)^2]/\Sigma[w(F_o^2)^2]]^{1/2}$, $w = 1/[\sigma^2(F_o^2) + (ap)^2 + bp]$, where $p = [\max(F_o^2, 0) + 2F_c^2]/3$.

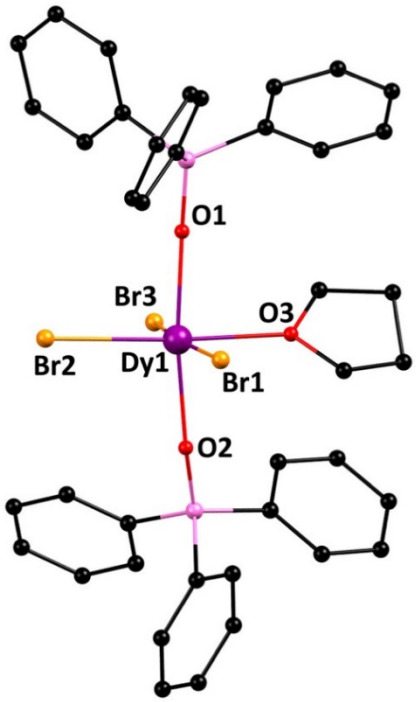

Figure S1. Crystal structure of **2**. H atoms were omitted for the sake of clarity. Colour scheme: Dy, purple; O, red; Br, orange; I, dark blue; C, black.

Table S2. Shape measures of the 6-coordinate lanthanide coordination polyhedra. The values in boldface indicate the closest polyhedron according to the Continuous Shape Measures.

Polyhedron[c]	**1**	**2**	**3**
HP-6	32.92	33.13	33.92
PPY-6	28.62	28.70	27.25
OC-6	**0.85**	**1.40**	**2.50**
TPR-6	16.68	16.70	15.85
JPPY-6	31.38	31.08	29.91

[c] Abbreviations: HP-6, hexagon; PPY-6, pentagonal pyramid; OC-6, octahedron; TPR-6, trigonal prism; JPPY-6, Johnson pentagonal pyramid J2.

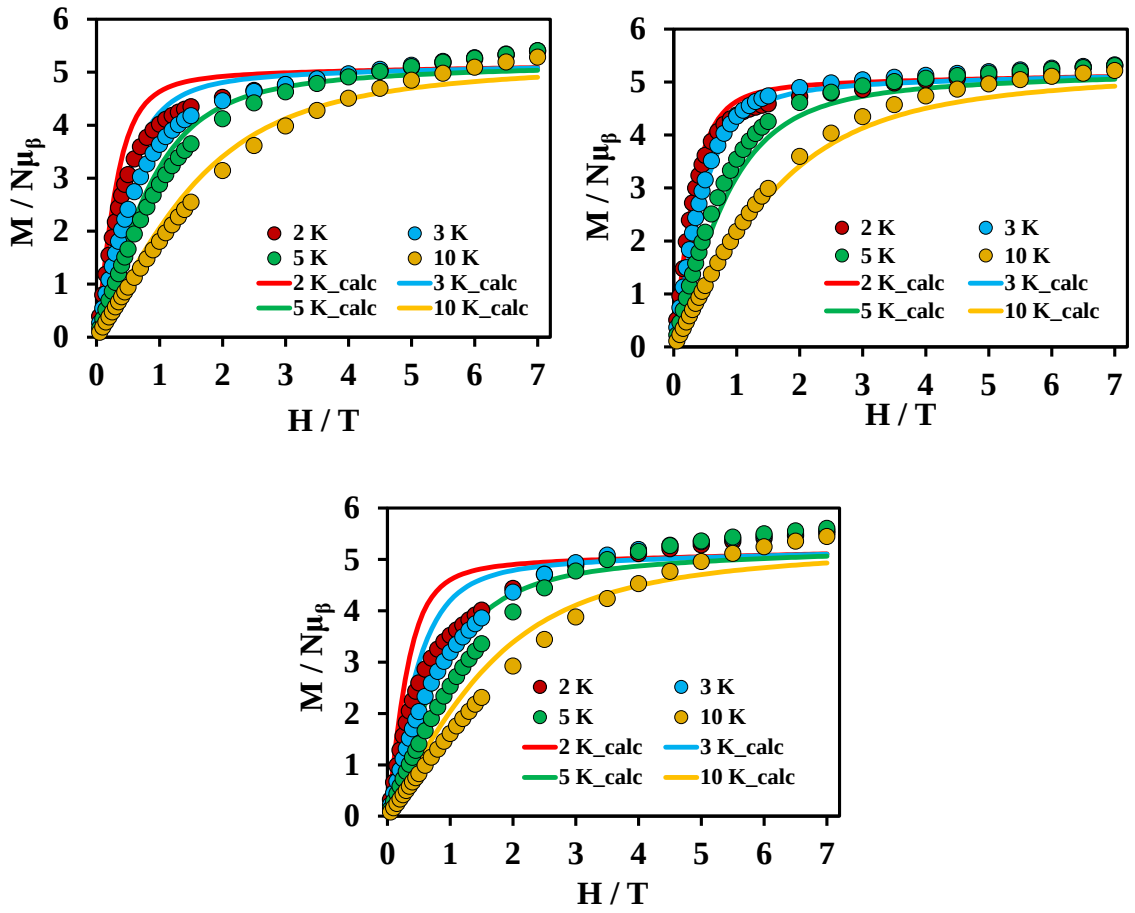

Figure S2. Plots of magnetization (M) vs field for (top left) **1** (Cl), (top right) **2** (Br) and (bottom) **3** (I) at different temperatures. The solid colour lines are *ab initio* calculated magnetization values.

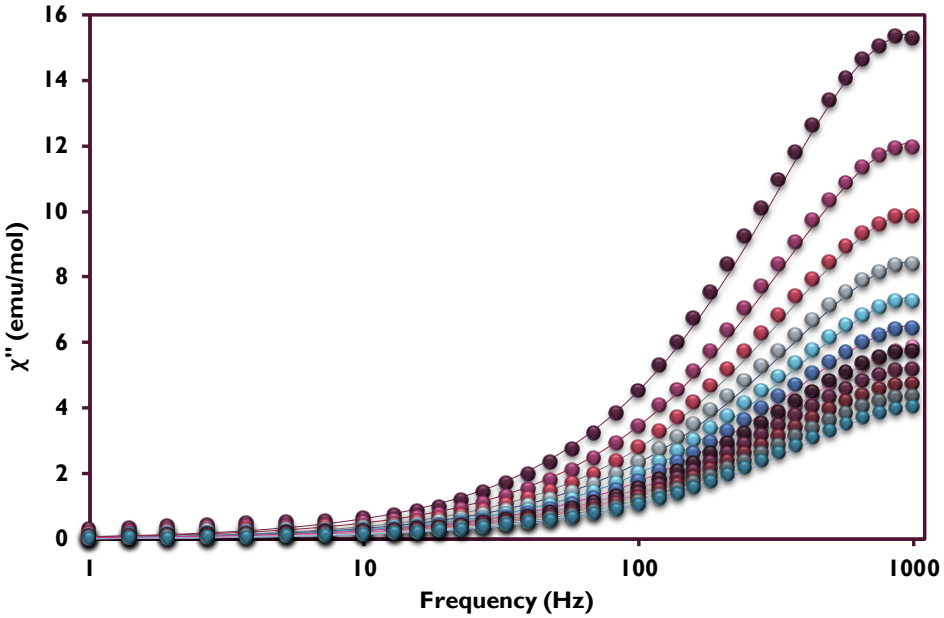

Figure S3. χ_M'' vs frequency for **2** at H_{dc} = 0 Oe.

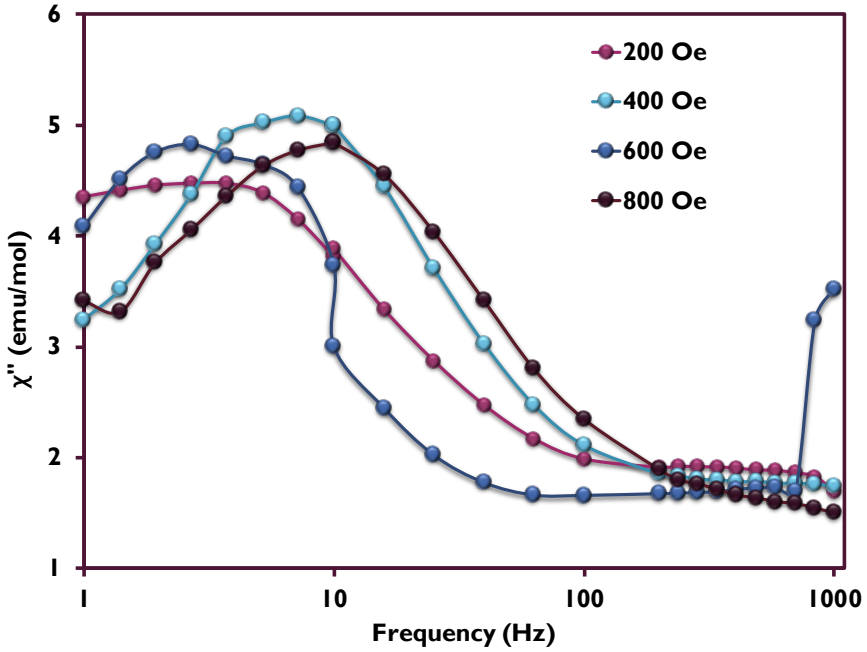

Figure S4. χ_M'' vs frequency plots for **2** at the indicated dc fields with fixed temperature showing the optimal field of 400 Oe.

Table S3. Cole-Cole fit values of **1** between 3 – 9 K under a *dc* field of 400 Oe and an *ac* measuring field of 2.0 Oe.

T / K	χ_S / cm^3 mol^{-1}	χ_t / cm^3 mol^{-1}	τ / s	α	Residual
3	38.12810	63.36470	0.16450	0.34536	6.02890
4	33.20780	46.32500	0.02300	0.13770	1.76546
5	28.88600	39.01020	0.00581	0.06898	1.82667
6	25.49500	33.86340	0.00188	0.04934	1.37825
7	22.83270	29.96930	0.00074	0.04560	1.21139
8	20.49450	26.95960	0.00032	0.07763	0.86000
9	17.16200	24.53340	0.00010	0.15754	0.69138

Table S4. Cole-Cole fit values of **2** between 5 – 20 K under a *dc* field of 400 Oe and an *ac* measuring field of 2.0 Oe.

T / K	χ_S / cm^3 mol^{-1}	χ_t / cm^3 mol^{-1}	τ / s	α	Residual
5	9.857320	27.857000	0.119471	0.138583	1.436230
6	8.406410	21.657800	0.049762	0.060141	0.728880
7	7.325590	18.585800	0.018465	0.049207	0.138288
8	6.510300	16.229100	0.008447	0.035752	0.109131
9	5.876750	14.423600	0.004450	0.022940	0.174869
10	5.348400	13.004800	0.002620	0.021212	0.088406
11	4.941820	11.856400	0.001681	0.018763	0.063990
12	4.594610	10.883900	0.001140	0.015339	0.056865
13	4.317420	10.054200	0.000815	0.009613	0.061781
14	4.087520	9.369620	0.000605	0.005153	0.053627
15	3.851320	8.745200	0.000459	0.006609	0.058911
16	3.628380	8.254680	0.000357	0.017138	0.045087
17	3.462260	7.796970	0.000281	0.017418	0.053467
18	3.283330	7.375190	0.000225	0.018758	0.043908
19	3.095950	7.012840	0.000179	0.024252	0.027232
20	2.985470	6.674650	0.000148	0.020934	0.032580

Computational Details

Using MOLCAS 8.0,[8] *ab initio* calculations were performed on the Dy(III) ions using their crystal structures. Relativistic effects were taken into account on the basis of the Douglas−Kroll Hamiltonian.[9] The spin-free eigenstates were achieved by the Complete Active Space Self-Consistent Field (CASSCF) method.[10] The basis sets were taken from the ANORCC library for the calculations. We employed the [ANO-RCC... 8s7p5d3f2g1h.] basis set[11] for Dy^{III} atoms, the [ANO-RCC...3s2p.] basis set for C atoms, the [ANO-RCC...2s.] basis set for H atoms, the [ANO-RCC...4s3p1d.] basis set for P atoms, the [ANO-RCC...4s3p2d1f.] basis set for O atoms, and the [ANO-RCC...5s4p2d1f.] basis set for the Cl, Br and I atoms. In the first step, we ran a guessorb calculation using the seward module to create the starting guess orbitals. Here, we included nine electrons across seven 4f orbitals of the Dy^{III} ion. Then using these guess orbitals, we chose the active space based on the number of active electrons in the number of active orbitals and carried out the SA-CASSCF calculations. Here, the Configuration Interaction (CI) procedure was computed for Dy^{III} ion and we considered twenty-one sextet excited states, two hundred and twenty-four quartet excited states and four hundred and eighty doublet excited states in the calculations to compute the anisotropy. All the excited states corresponding to each multiplet of ions were computed in the CASSCF module. After computing these excited states, we mixed all the low-lying excited states (<50,000 cm^{-1}) using the RASSI-SO[12] module to calculate the spin-orbit coupled states. Moreover, these computed SO states were considered in the SINGLE_ANISO[13] program to compute the *g*-tensors. The *g*-tensors for the Kramers doublets of Dy(III) were computed based on the pseudospin S = ½ formalism.[13] Crystal-field (CF) parameters were extracted using the SINGLE_ANISO code, as implemented in MOLCAS 8.0. The CF parameters for all three complexes were analysed for deeper insight into the mechanism of magnetic relaxation. The corresponding crystal field Hamiltonian is given in equation:

$$\hat{H}_{CF} = \sum \sum_{k=-q}^{q} B_k^q \tilde{O}_k^q \quad \text{..... Eq.1}$$

where B_k^q is the crystal field parameter, while O_k^q is the Steven's operator.

We used the Loprop charges to determine the direction of magnetic anisotropy which is a static property that can be computed like a charge, a component of the dipole moment, or an exchange-hole dipole moment,[14] is localized by transforming the property of two centers.[15]

Table S5. The *g*-tensor for the eight lowest Kramer's doublets in **1** – **4**.

KDs		**1**	**2**	**3**	**4**
1	g_x	0.0545	0.0062	0.2921	0.0016
	g_y	0.1326	0.0111	1.0878	0.0031
	g_z	19.7570	19.9166	19.0160	19.9201
2	g_x	1.7250	0.6104	0.4212	0.2141
	g_y	2.7924	0.6506	0.7321	0.2620
	g_z	16.9242	16.4640	18.3411	16.7417
3	g_x	2.9973	0.5484	3.6154	2.8995
	g_y	6.1035	1.8080	5.8691	3.8349
	g_z	10.0641	16.7414	11.7744	14.9433
4	g_x	6.5252	3.7515	7.9604	1.9199
	g_y	5.8311	6.4397	6.0995	5.1779
	g_z	0.8584	10.3210	0.0779	10.2950
5	g_x	1.1603	2.2976	2.4533	2.6117
	g_y	2.1501	3.9149	3.8144	4.3364
	g_z	7.9671	10.8799	10.4990	9.8564
6	g_x	10.9430	9.0979	0.3701	9.7931
	g_y	7.0435	7.1539	1.5891	5.9341
	g_z	1.3336	1.5135	14.5053	0.0972
7	g_x	1.0866	1.7423	0.1030	0.5766
	g_y	3.4881	5.7748	0.2249	4.3183
	g_z	10.7743	10.9951	18.0732	12.4676
8	g_x	1.4520	0.3335	0.8733	1.4159
	g_y	4.1679	2.9842	1.8175	3.4865
	g_z	14.5386	15.9010	16.3762	15.4838

Table S6. RASSI energies of the lowest spin-orbit states (cm^{-1}) of each Dy center in **1** – **4**.

1	**2**	**3**	**4**

0.000	0.000	0.000	0.000
147.329	234.906	46.129	272.517
196.254	332.299	217.089	427.299
225.750	358.459	312.148	475.715
360.885	465.264	460.695	586.128
394.610	511.852	573.250	612.742
435.281	551.724	591.289	665.306
474.303	591.700	641.926	694.866
3214.547	3110.300	3103.525	3128.944
3236.768	3289.237	3143.900	3334.681
3260.508	3351.325	3251.771	3424.887
3282.747	3382.703	3323.951	3465.475
3322.972	3405.317	3410.108	3514.336
3330.645	3451.893	3486.435	3566.792
5733.620	3459.539	3559.136	3585.160
5780.697	5775.419	5742.834	5808.588
5808.953	5870.065	5778.545	5920.709
5824.624	5895.627	5837.304	5964.909
5869.639	5935.788	5906.179	6022.871
5898.187	5997.824	5988.644	6100.313
6036.142	6047.239	6122.648	6167.919
7947.462	7992.074	7931.637	8035.394
7974.418	8035.009	7974.895	8085.479
8018.601	8065.369	8037.929	8137.017
8092.776	8141.616	8116.790	8234.355
9628.803	8231.375	8281.807	8341.396
9647.300	9717.451	9659.154	9760.560
9684.516	9740.895	9681.174	9790.119
9691.002	9755.018	9756.407	9811.328
9728.257	9811.732	9771.468	9811.328
9752.237	9827.469	9799.972	9878.436
9765.105	9841.844	9817.966	9894.228
9780.614	9874.406	9847.228	9918.186
9796.834	9896.941	9891.421	9958.869
9904.941	9912.041	9912.858	9974.026
11058.245	10027.480	10065.218	9993.781
11170.354	11112.769	11044.455	10130.609
11266.087	11315.746	11256.821	11143.834
11855.317	11378.841	11455.121	11409.523
	11954.916	11932.444	

11873.771	11981.691	11956.741	11474.429
11897.319	11993.228	11970.310	12020.080
11915.377	12019.382	12023.489	12045.717
11953.755	12063.477	12050.638	12053.274
12024.544	13692.585	13671.511	12084.536
13586.749	13785.336	13764.552	12144.923
13685.801	13803.143	13794.577	13756.063
13698.654	13834.838	13822.000	13847.930
13729.666	15107.901	15087.784	13866.290
15003.904	15182.415	15162.850	13903.820
15080.195	15192.104	15184.156	15167.989
15086.225	16150.849	16129.248	15246.151
16048.794	16160.826	16153.061	15255.918
16055.533	16747.352	16734.434	16210.666
16642.395	38949.552	38848.386	16223.284
38908.273	38989.338	38985.922	16809.617
38935.972	39071.868	39102.031	38881.047
38983.335	39242.419	39188.946	38944.059
39068.794	40328.282	40253.086	39050.571
40275.967	40510.621	40405.980	39313.457
40384.378	40615.803	40764.745	40296.160
40449.006	41450.687	41464.604	40525.482
41344.081	41513.900	41540.734	40700.137
41379.854			41555.094

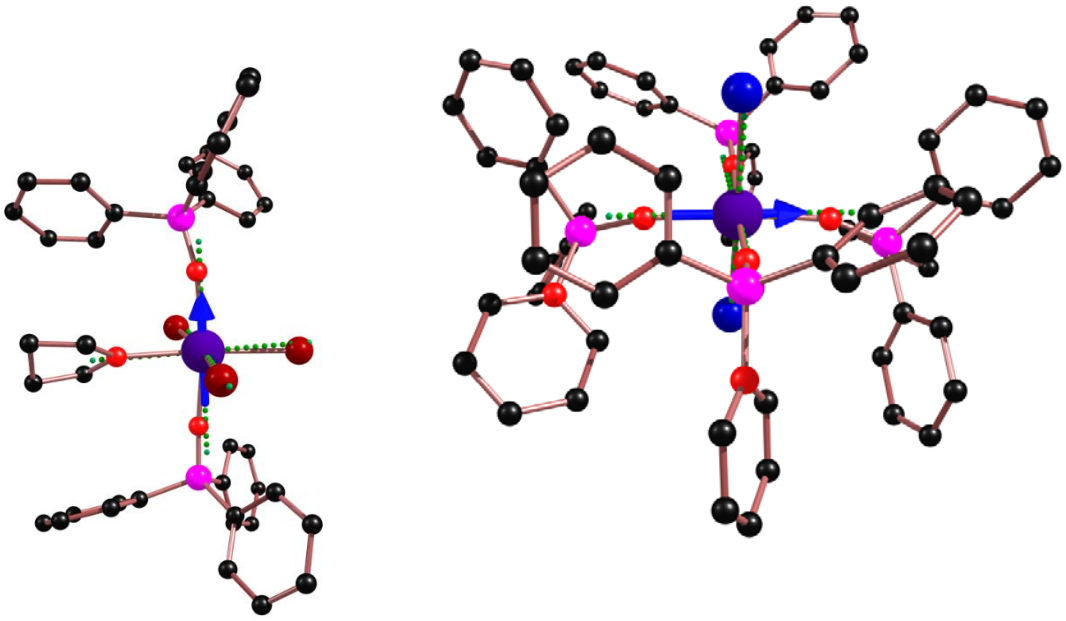

Figure S5. The orientation of the principle magnetization g_{zz}, g_{xx}, and g_{yy} axes (dotted green lines) and the main magnetic anisotropy directions (blue arrows) of the Dy^{III} ions for (left) **2** (the same orientations are applicable to **1**); and (right) **3**. Colour scheme: Dy^{III}, purple; P, pink; Br, dark red; I, navy blue; O, red; N, blue.

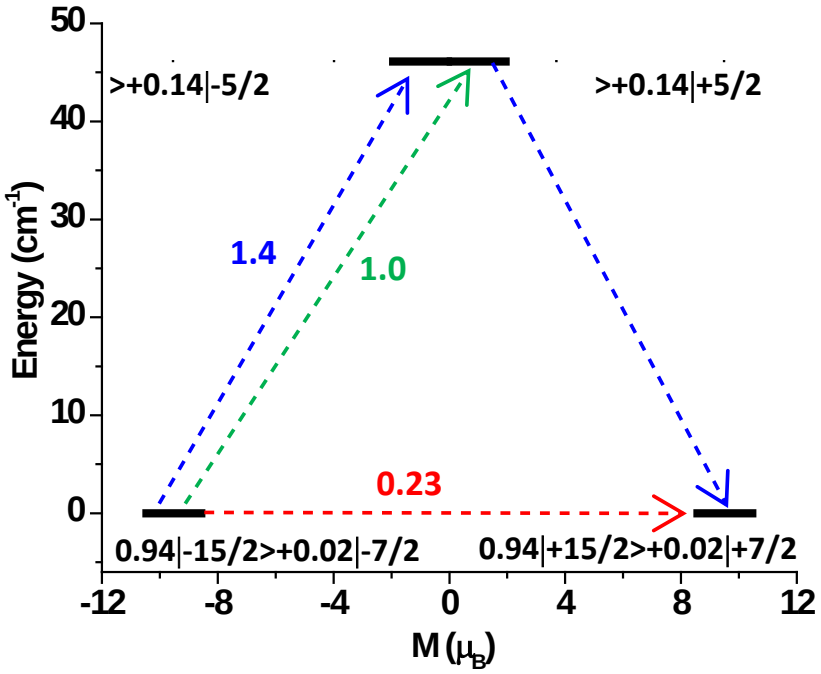

Figure S6. Ab initio computed magnetization blocking barrier for **3**.

Table S7. SINGLE_ANISO computed crystal field parameters for **1** – **4**. The major components in the Table are in bold. B_k^q is the crystal field parameter and O_k^q is the extended Stevens operator. The quantization axis is chosen to be the main magnetic axis of the ground pseudo-Doublet.

k	q	B_k^q	B_k^q	B_k^q	B_k^q
		1	**2**	**3**	**4**
2	-2	0.08	-0.03	0.08	0.14
	-1	**-1.20**	-0.72	-0.74	-0.75
	0	**-1.20**	**-2.22**	**-1.87**	**-3.04**
	1	0.19	1.0	**0.12**	**0.40**
	2	**0.47**	**-0.33**	**4.67**	**-1.04**
4	-4	0.003	-0.006	0.0003	0.01
	-3	0.002	-0.006	0.02	-0.005
	-2	0.0001	0.001	0.0002	-0.0003
	-1	0.009	0.002	0.01	0.003
	0	-0.01	-0.01	-0.01	-0.01
	1	-0.0006	-0.006	-0.001	-0.002
	2	0.0002	0.002	-0.01	0.002
	3	0.002	0.01	0.002	0.008
	4	0.04	-0.003	-0.04	-0.03

References:

1. Bruker-AXS, *Journal*, 2015.
2. G. M. Sheldrick, *SADABS*, 1996.
3. G. M. Sheldrick, *Acta Crystallogr. Sect. A, Found. and Adv.*, 2015, **71**, 3-8.
4. G. M. Sheldrick, *Acta crystallogr. Sect. C, Struc. Chem.*, 2015, **C71**, 3-8.
5. O. V. Dolomanov, L. J. Bourhis, R. J. Gildea, J. A. K. Howard and H. Puschmann, *J. Appl. Crystallogr.*, 2009, **42**, 339-341.
6. W. Pennington, *J. Appl. Crystallogr.*, 1999, **32**, 1028-1029.

7. C. F. Macrae, P. R. Edgington, P. McCabe, E. Pidcock, G. P. Shields, R. Taylor, M. Towler and J. van de Streek, *J. Appl. Crystallogr.*, 2006, **39**, 453-457.

8. F. Aquilante, J. Autschbach, R. K. Carlson, L. F. Chibotaru, M. G. Delcey, L. D. Vico, I. F. Galván, N. Ferré, L. M. Frutos, L. Gagliardi, M. Garavelli, A. Giussani, C. E. Hoyer, G. L. Manni, H. Lischka, D. Ma, P. Å. Malmqvist, T. Müller, A. Nenov, M. Olivucci, T. B. Pedersen, D. Peng, F. Plasser, B. Pritchard, M. Reiher, I. Rivalta, I. Schapiro, J. Segarra-Martí, M. Stenrup, D. G. Truhlar, L. Ungur, A. Valentini, S. Vancoillie, V. Veryazov, V. P. Vysotskiy, O. Weingart, F. Zapata and R. Lindh, *J. Comput. Chem.*, 2016, **37**, 506-541.

9. B. A. Hess, C. M. Marian, U. Wahlgren and O. Gropen, *Chem. Phys. Lett.*, 1996, **251**, 365-371.

10. B. O. Roos and P.-A. Malmqvist, *Phys. Chem. Chem. Phys.*, 2004, **6**, 2919-2927.

11. B. O. Roos, R. Lindh, P.-A. Malmqvist, V. Veryazov, P.-O. Widmark and A. C. Borin, *J. Phys. Chem. A*, 2008, **112**, 11431-11435.

12. P. A. Malmqvist, B. O. Roos and B. Schimmelpfennig, *Chem. Phys. Lett.*, 2002, **357**, 230-240.

13. L. F. Chibotaru and L. Ungur, *J. Chem. Phys.*, 2012, **137**, 064112-064122.

14. L. Gagliardi, R. Lindh and G. Karlström, *J. Chem. Phys.*, 2004, **121**, 4494-4500.

15. (a) B. Wang, S. L. Li and D. G. Truhlar, *J. Chem. Theory. Comput.*, 2014, **10**, 5640-5650; (b) S. K. Langley, K. R. Vignesh, K. Holton, S. Benjamin, G. B. Hix, W. Phonsri, B. Moubaraki, K. S. Murray and G. Rajaraman, *Inorganics*, 2018, **6**.